Statistical mechanics of vacancy and interstitial strings in hexagonal columnar crystals

Shilpa Jain and David R. Nelson
Lyman Laboratory of Physics, Harvard University, Cambridge, Massachusetts 02138
(Received 2 April 1999)

Columnar crystals contain defects in the form of vacancy-interstitial loops or strings of vacancies and interstitials bounded by column ''heads'' and ''tails.'' These defect strings are oriented by the columnar lattice and can change size and shape by movement of the ends and by forming kinks along the length. Hence an analysis in terms of directed living polymers [S. A. Safran, *Statistical Thermodynamics of Surfaces, Interfaces, and Membranes* (Addison-Wesley, Reading, MA, 1994), Sec. 8] is appropriate to study their size and shape distribution, volume fraction, etc. If the entropy of transverse fluctuations overcomes the string line tension in the crystalline phase, a string proliferation transition occurs, leading to a supersolid phase [E. Frey, D. R. Nelson, and D. S. Fisher, Phys. Rev. B **49**, 9723 (1994); see also J. Prost, Liq. Cryst. **8**, 123 (1990)]. We estimate the wandering entropy and examine the behavior in the transition regime. We also calculate numerically the line tension of various species of vacancies and interstitials in a triangular lattice for power-law potentials as well as for a modified Bessel function interaction between columns such as occurs in the case of flux lines in type-II superconductors or long polyelectrolytes in an ionic solution. We find that the centered *interstitial* is the lowest-energy defect for a very wide range of interactions; the symmetric vacancy is preferred only for extremely short interaction ranges.

PACS number(s): 61.30.Cz, 61.30.Jf, 64.60.Cn

I. INTRODUCTION

The physics of columnar crystals is relevant to the Abrikosov lattice of flux lines in type-II superconductors and liquid crystalline materials like concentrated phases of long polymers or discotics. The stability of the columnar crystal has been investigated, and various mechanisms proposed for its melting. Conventional melting, which arises when phonon displacements reach a fixed fraction of the lattice constant, can easily be located via the Lindemann criterion [3,4]. Melting destroys the two-dimensional crystalline order perpendicular to the columns leading to a nematic liquid of lines or columns, which is entangled at sufficiently high densities.

Crystal defects play an important role above the melting transition. If edge dislocations in the crystal proliferate, they drive the shear modulus to zero, leading to a liquidlike shear viscosity. However, dislocations alone cannot destroy the sixfold orientational order of the triangular lattice in a two-dimensional cross section. Thus, provided disclination lines do not also proliferate, the resulting liquid of lines is hexatic, not isotropic [5]. The screw component of the unbound dislocations leads to entanglement. A finite concentration of unbound disclinations superimposed on the hexatic liquid leads to isotropic in-plane order.

Another kind of transition is brought about by vacancy-interstitial line defects in columnar crystals composed of long, continuous lines. As discussed in Ref. [2], under suitable conditions (such as high field and small interlayer coupling in layered superconductors), it can become favorable for these line defects to proliferate. If this happens at a temperature T_d below the melting temperature T_m, then the phase that exists between T_d and T_m will be simultaneously crystalline and highly entangled. In the boson analogy of an aligned system of lines, where the lines represent two-dimensional bosons traveling in the ''timelike'' axial ($\hat{\mathbf{z}}$) direction [3], such a phase is analogous to the supersolid phase of the bosonic system, which incorporates vacancies and interstitials in its ground state. This entangled solid melts into an entangled liquid or an entangled hexatic at even higher temperatures.

The proliferation of vacancy or interstitial strings could also affect a crystal-to-hexatic transition mediated by dislocations. Dislocations in the columnar crystalline geometry are normally constrained to lie in the vertical plane formed by their Burgers vector and the $\hat{\mathbf{z}}$ axis, because a dislocation in a two-dimensional cross section can move along the columnar axis only through glide parallel to its Burgers vector. Transverse motion (climb) would require it to absorb or emit vacancies or interstitials. This becomes possible in the supersolid phase, thus allowing dislocation loops to take on arbitrary nonplanar configurations which would have to be included in the treatment of Ref. [5] to study melting out of a supersolid phase [6].

Vacancy and interstitial strings in a columnar crystal tend to be lines themselves because of the continuity of the columns. If the columns are constrained to be continuous across the entire sample (as is the case for vortex lines in type-II superconductors), these defects must either thread the entire sample (Fig. 1) or appear in vacancy and interstitial pairs forming loops (Fig. 2) [2]. The situation is different, however, for finite-length polymers, or columns of discotic liquid crystal molecules which can break and reform freely. As illustrated in Fig. 3(a), a slice through a low temperature configuration in a polymer columnar crystal (with translational order perpendicular to the column axis but not parallel to it) would consist of tightly bound polymer ''heads and tails.'' At higher temperatures, however, the heads and tails will separate, either moving apart to form a vacancy string or sliding past each other to form a line of interstitials [Fig. 3(b)] [7]. In columnar discotic crystals with similar translational order, ''heads'' and ''tails'' are absent at low tempera-

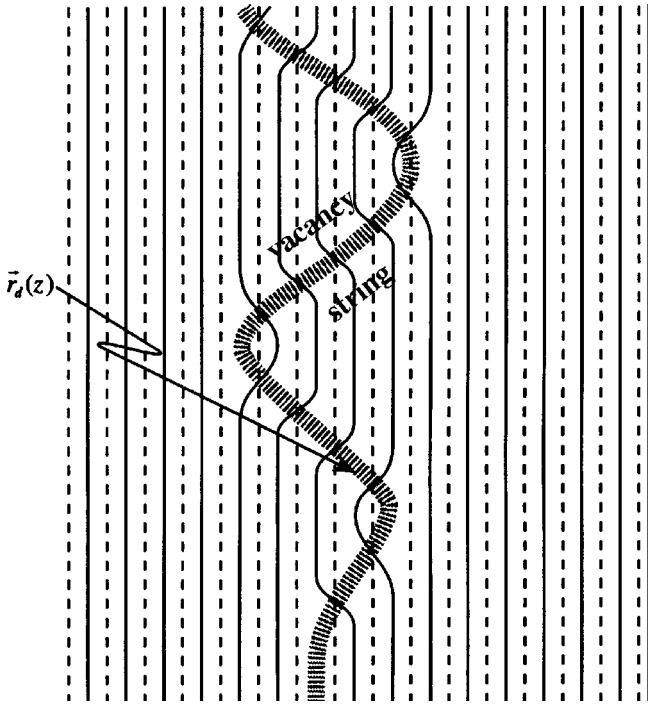

FIG. 1. Vacancy string $\mathbf{r}_d(z)$ (thick dashed curve) meandering through a columnar crystal. Dashed lines represent columns just above or below the plane of the figure. (Taken from Ref. [2].)

tures, but appear spontaneously when vacancy and interstitial strings are excited (Fig. 4). (Head and tail defects appear superficially like dislocations in the cross sections shown in Figs. 3 and 4. A three-dimensional analysis of lines and columns in neighboring sheets like that shown in Figs. 1 and 2 is necessary to clearly reveal that these are strings of vacancies and interstitials.)

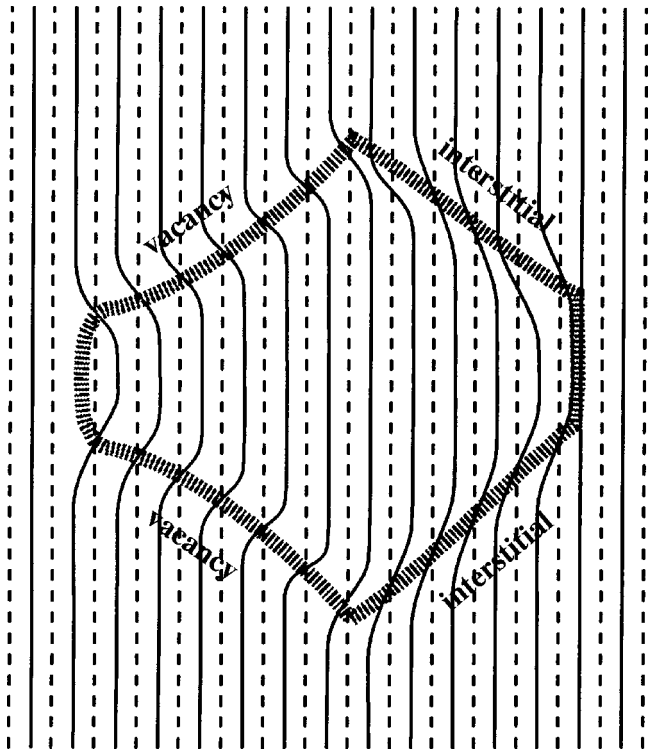

FIG. 2. Vacancy-interstitial loop in a columnar crystal. Dashed lines represent columns just above or below the plane of the figure. (Taken from Ref. [2].)

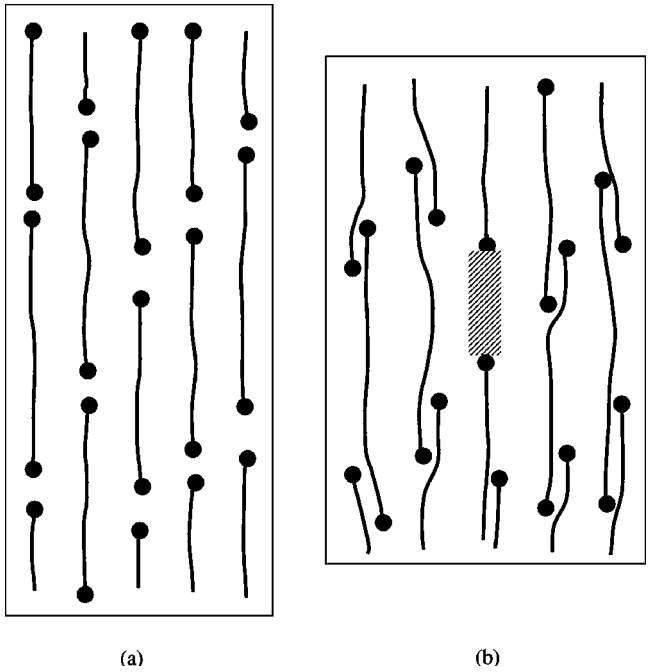

FIG. 3. Formation of vacancy or interstitial strings by sliding of polymers within columns in a columnar crystal of finite-length polymers.

Unlike dislocation lines, these strings (and loops) are not constrained to be planar: the lines can jump to any neighboring lattice site as they traverse the crystal. Several horizontal jumps connecting a head to a tail are shown in Fig. 5. Note that *leftward* deflections of the vacancy segment connecting a head to a tail are accompanied by *rightward* deflections of the lines or columns themselves. A typical string can be approximated by an alternating sequence of straight segments

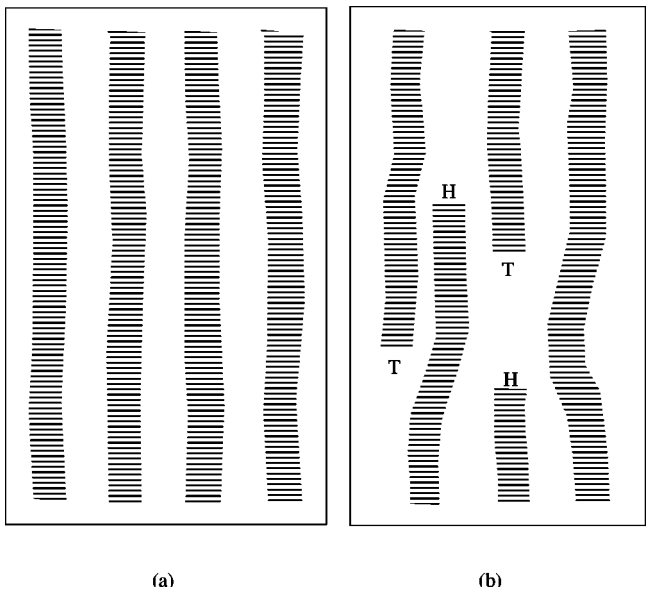

FIG. 4. Formation of vacancy or interstitial strings in a discotic columnar crystal by columns sliding past each other, or incurring gaps.

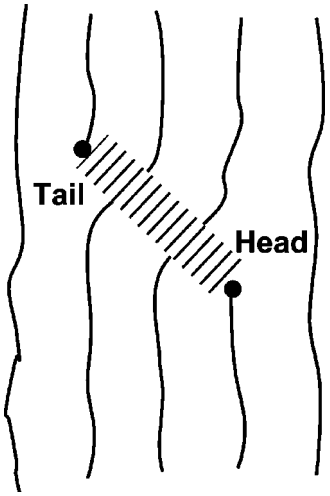

FIG. 5. Illustration of a vacancy string (thick dashed curve) joining a column head to another column's tail in a columnar crystal composed of long-chain polymers.

and kinks joining the head of one column or polymer chain to the tail of another (see Fig. 6).

These line defects are topologically stable in the (2+1)-dimensional columnar geometry, as are the corresponding point defects in two dimensions. Although a line defect in a (1+1)-dimensional geometry would be pinched off by relaxation of the neighboring columns into or away from it, such relaxation is not possible in the (2+1)-dimensional case, as each (1+1)-dimensional plane has to stay commensurate with its neighboring planes. A translation of columns in the neighborhood of the line defect can only translate the defect laterally.

Vacancy and interstitial strings are suppressed at low temperatures because they have a finite line tension, and hence an energy proportional to their length. At higher temperatures, heads and tails can move apart, forming variable-length strings that wander or ''diffuse'' perpendicular to their length by forming kinks. These strings thus resemble living polymers [1], except that they are directed, on average, along the $\hat{\mathbf{z}}$ axis. In polymer crystals, the number of such strings is determined by the fixed concentration of heads and tails. In columnar discotic crystals, heads and tails can be created freely, and it is appropriate to treat their statistical

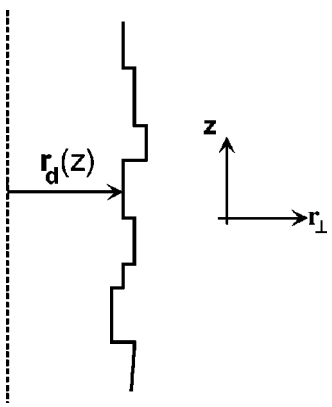

FIG. 6. Schematic of a defect string (composed of straight segments and kinks) wandering through the columnar crystal.

mechanics in a grand canonical ensemble by introducing a head and/or tail fugacity, similar to the fugacity that controls defect concentrations in theories of vortex or dislocation unbinding transitions [8]. We assume here that we can treat polymer crystals using the same formalism provided we tune the head or tail fugacity to achieve the fixed concentration determined by the mean polymer length. Long polymers imply a dilute distribution of heads and tails. We exclude, for simplicity, the possibility of hairpin excitations in polymer systems, which can be regarded as doubly quantized interstitial excitations leading to a higher energy. As we shall see, the sharp defect proliferation transition discussed in Ref. [2] is blurred when there is a finite concentration of heads and tails in equilibrium.

Given an appropriate combination of parameters, namely, low line tension combined with head and/or tail and kink energies comparable to the temperature, the entropy of diffusion of the strings can overcome the line tension and lead to string proliferation, allowing heads and tails to separate to arbitrarily large distances. As in its bosonic counterpart, there exists off-diagonal long-range order in this phase, represented by

$$\lim_{|\mathbf{r}'_\perp-\mathbf{r}_\perp|\to\infty} \langle \psi(\mathbf{r}_\perp,z)\psi^*(\mathbf{r}'_\perp,z')\rangle \neq 0 \qquad (1.1)$$

where ψ and ψ^* are head and tail ''destruction'' and ''creation'' operators [3], implying entanglement of lines on a macroscopic scale. If defects are absent or appear only in closed loops, the expression above will vanish as $|\mathbf{r}'_\perp-\mathbf{r}_\perp| \to\infty$. Once defects proliferate, a line can wander to any other column and Eq. (1.1) has a finite limit. A crystal with proliferating vacancies and interstitials is an incommensurate phase—the magnitude of the smallest reciprocal vector $G = 4\pi/\sqrt{3}a_0$ is no longer related to the areal density in the obvious way as $\rho = \sqrt{3}G^2/8\pi^2$ because the density differs from its defect-free value $\rho_0 = 2/\sqrt{3}a_0^2$ (a_0 being the lattice constant of the triangular lattice in cross section). All crystals of pointlike atoms or molecules are trivially ''incommensurate'' in this sense—the corresponding pointlike vacancies and interstitials proliferate at any finite temperature. It is the anomalous suppression of vacancies and interstitials and their organization into lines at low temperatures in columnar crystals that makes these materials unusual.

The discrepancy between the density of columns as inferred from x-ray measurements of the lattice constant, and the molar concentration of the columns, gives a measure of the volume fraction of vacancy or interstitial defects in the crystal. In experiments performed by Albouy *et al.* [9] on hexagonal columnar phases of thermotropic mesogens as discotic units, measurements indicate a significant departure between these two values at temperatures close to the hexatic $\rightarrow$ nematic transition and above. At the transition itself, there is a jump in the defect volume fraction of order 1/100. As the head and/or tail fugacity of defect strings approaches infinity, we expect to see a sharp second-order transition with $\rho - \rho_0 \propto T - T_d$ [3].

One of the conditions that makes proliferation of line defects energetically favorable is low shear modulus. If the supersolid phase appears in a narrow region close to the melting of the hexagonal columnar crystalline phase, it might

appear very similar experimentally to the hexatic phase. Evidence of a hexatic phase in high-density DNA solutions has been found in experiments by Podgornik *et al.* [10], using structural probes coupled with osmotic stress measurements.

In this paper we apply the physics of directed lines to vacancy and interstitial strings. With this in mind, we briefly review the elasticity theory of these systems in the next section. In Sec. III we model a single string and estimate its transverse wandering. The form of this wandering is unchanged by coupling to phonon distortions of the lattice, as shown in Appendix A. So is its magnitude, as calculated in Appendix B. In Sec. IV we apply the statistical mechanics of living polymers to an ensemble of directed strings and calculate their volume fraction, average length, etc., in the noninteracting limit. A simple quadratic-interaction model is presented in Sec. V, similar to the one discussed via the boson mapping in Ref. [3], and we reproduce the results therein. Numerical calculations of the line tensions of various species of defects are presented in Sec. VI. The interaction potentials considered are repulsive and monotonic; we study simple power laws as well as a screened Debye-Hückel interaction. We find many metastable species of vacancies. However, the lowest-energy defect is always found to be the one with the highest symmetry in its category. For very short range interactions, this is the symmetric vacancy (V_6), whereas for most interactions the centered interstitial (I_3) is most favored. Appendix D contains details of the Ewald summation calculations for the potentials considered here.

II. REVIEW OF ELASTICITY THEORY

Before discussing defects in a columnar crystal, we review the aspects of elasticity theory common to all the systems mentioned in the Introduction. We consider lines or columns aligned along a common direction ($\hat{\mathbf{z}}$) up to thermal fluctuations, with crystalline order in any cross section perpendicular to the columnar axis. In the case of flux lines, the average direction of alignment is imposed by an external field ($\mathbf{H}=H\hat{\mathbf{z}}$) and local deviations from this direction cost energy. With columnar crystals of long-chain molecules composed of covalently bonded nematogens or disk-shaped molecules cylindrically stacked via hydrogen bonds, or amphiphilic molecules in cylindrical micellar aggregates, the columnar axis represents spontaneously broken rotational symmetry. Therefore local deviations from the alignment direction are not penalized, but undulations of the column are. The rotational symmetry can, however, be broken by imposing an external field. In addition, the two-dimensional crystalline order resists shear and areal deformations perpendicular to the $\hat{\mathbf{z}}$ axis.

Low-energy fluctuations of the system can be described by a ''continuum'' model that works for small-amplitude, long-wavelength deformations [11,3,12]. The important fluctuations in this limit can be characterized by a two-dimensional (2D) displacement field $\mathbf{u}(\mathbf{r}_\perp,z)$, representing the average deviation of lines in the (x,y) plane in a small region centered at $(\mathbf{r}_\perp,z)$. With it can be associated a local areal density change $\delta\rho/\rho_0=-\boldsymbol{\nabla}_\perp\cdot\mathbf{u}$ ($\rho_0=2/\sqrt{3}a_0^2$) and a local nematic director $\hat{\mathbf{n}}=\hat{\mathbf{z}}+\mathbf{t}$, with $\mathbf{t}\equiv\partial\mathbf{u}/\partial z$. The free energy of the system is a sum of nematic and crystalline contributions:

$$\mathcal{F}=\mathcal{F}_{nematic}+\mathcal{F}_{crystal}. \tag{2.1}$$

To the lowest order in the fluctuations, these are given by

$$\mathcal{F}_{nematic}=\frac{1}{2}\int d^3r[K_1(\boldsymbol{\nabla}_\perp\cdot\mathbf{t})^2+K_2(\boldsymbol{\nabla}_\perp\times\mathbf{t})^2+K_3(\partial_z\mathbf{t})^2] \tag{2.2}$$

and

$$\mathcal{F}_{crystal}=\int dz\int d^2\mathbf{r}_\perp\left[\mu\,u_{ij}^2+\frac{1}{2}\lambda\left(\frac{\delta\rho}{\rho_0}\right)^2\right], \tag{2.3}$$

where K_1, K_2, and K_3 are the Frank constants for splay, twist, and bend, respectively, and λ and μ are the Lamé coefficients. The matrix $u_{ij}=(\partial_i u_j+\partial_j u_i)/2$ is the linearized 2D strain field. In the presence of an external field $H\hat{\mathbf{z}}$, one should add to $\mathcal{F}$

$$\mathcal{F}_{ext}=\frac{1}{2}\chi_a H^2\int dz\int d^2r_\perp|\mathbf{t}|^2, \tag{2.4}$$

where χ_a is the anisotropic part of the susceptibility [12].

The last two contributions to $\mathcal{F}$ are quadratic in the derivatives, and can be rewritten as

$$\mathcal{F}_{crystal}+\mathcal{F}_{ext}=\frac{1}{2}\int d^3r[c_{11}(\boldsymbol{\nabla}_\perp\cdot\mathbf{u})^2+c_{66}(\boldsymbol{\nabla}_\perp\times\mathbf{u})^2+c_{44}(\partial_z\mathbf{u})^2]+(\text{surface terms}) \tag{2.5}$$

where $c_{11}\equiv\lambda+2\mu$, $c_{66}\equiv\mu$, and $c_{44}\equiv\chi_a H^2\rho$. The surface terms become important when there are defects within the bulk of the crystal, like vacancy and interstitial strings, represented by cuts joining column-end singularities in the field $\mathbf{u}(\mathbf{r}_\perp,z)$. Evaluating these terms over a cylindrical surface enclosing such a string yields the energy cost of the defect string: a line tension $\tau_z\approx\mu a^2$ due to the elastic distortion around the string, in addition to a core energy E_c per unit length (of the same order of magnitude) within the cylindrical core.

$\mathcal{F}_{nematic}$ can be further simplified if, as is often the case with nematic polymers, the splay and twist constants are small in comparison to the bend constant. Specifically, if K_1 and K_2 satisfy $K_{1,2}a_0^{-1}/\sqrt{K_3c_{11}}\ll 1$ [4], then they can be neglected. For long-wavelength distortions along the columnar axis, the dominant free energy contribution is then $K_3(\partial_z^2\mathbf{u})^2$ in the absence of an external field. K_3 can be simply related to the persistence length l_P of the polymer as $K_3=k_BTl_P\rho$.

The statistical mechanics of defects in polymer liquid crystals has been discussd in detail by Selinger and Bruinsma [13,14]. The presence of defects imposes a deformation on the $T=0$ equilibrium configuration. In the case of a semi-infinite vacancy or interstitial string with a head or tail at the origin, this distortion follows from minimization of the free energy above with respect to $\mathbf{u}(\mathbf{r}_\perp,z)$ under the constraint

$$\boldsymbol{\nabla}_\perp\cdot\mathbf{u}=\pm\rho_0^{-1}\delta(\mathbf{r}_\perp)\theta(z)+(\text{nonsingular terms}), \tag{2.6}$$

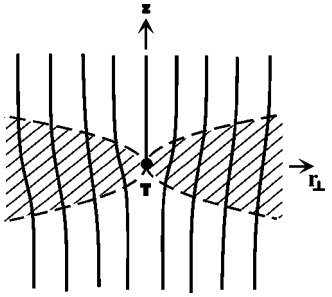

FIG. 7. Distortion induced by a column end in the neighboring columnar crystalline matrix. The distortion is confined to a vertical extent $|z| < \sqrt{\lambda_L r_\perp}$ (shaded region) around the column end.

where the $\pm$ sign refers to a column tail or head located at the origin. Since the planar distortion about a string has azimuthal symmetry in the continuum approximation, $\boldsymbol{\nabla}_\perp \times \mathbf{u} = \mathbf{0}$. Hence, the only relevant terms in the free energy are the bend and bulk distortion terms (neglecting splay). The resulting distortion around the column end spans a parabolic region about the radial direction (see Fig. 7) defined by

$$z^2 \lesssim \lambda_L r_\perp \tag{2.7}$$

where $\lambda_L = \sqrt{K_3/c_{11}}$ is the length scale relating the distortions parallel and perpendicular to $\hat{\mathbf{z}}$.

Selinger and Bruinsma also calculate the interaction energy between two column ends by superimposing the distortion created by each. They find the interesting result that a head and tail in a *nematic* medium attract weakly if they fall within each other's region of influence, as just described, but repel otherwise. However, in a columnar crystal (with nonzero shear modulus), the interaction is always a strong attractive linear potential due to the finite line tension associated with the string of distortions joining a head to a tail.

III. WANDERING OF A SINGLE STRING

Consider a single vacancy or interstitial string in a hexagonal columnar crystal of, say, polymer strands with lattice constant a_0 and monomer spacing c along the columnar axis $\hat{\mathbf{z}}$. For a discotic columnar liquid crystal, c is the spacing between oblate molecules along the column axis. For a flux line in a layered type-II superconductor with magnetic field perpendicular to the layers, c is the layer spacing. If the string is vertical, the energy per unit length τ_z is of the order of μa_0^2 (see Sec. II) where μ is the in-plane shear modulus of the crystal. For a horizontal string, $\tau_\perp = \varepsilon_k / a_0$ where the kink energy $\varepsilon_k \sim \kappa^{1/4}\mu^{3/4}a_0^2$ [3], $\kappa \equiv K_3/\rho$ being the bending rigidity. The ratio is $\tau_\perp/\tau_z \sim (\kappa/\mu)^{1/4}/a_0 \sim l^*/a$ where l^* is the kink size. Typically $l^* \gg a_0$, so that the strings are predominantly vertical, with few kinks. For flux lines, on the other hand, the kink energy is $g^{1/2}\mu^{1/2}a_0$ with $g \equiv c_{44}/\rho$, where c_{44} is the tilt modulus and ρ is the areal line density. The ratio is then $(g/\mu)^{1/2}/a_0$. In highly anisotropic layered superconductors, this ratio can be small, favoring large, nearly horizontal defect excursions. We will for now work with nearly vertical strings, allowing for a gas of kinks sufficiently dilute so that the interaction between kinks can be ignored (see Fig. 6). We thus assign to a string of vertical extent l and n_k kinks an energy $l\tau + n_k\varepsilon_k + 2\varepsilon_0$ where $\tau \equiv \tau_z$ and ε_0 is the energy of a polymer end. We expect that the results for defects with a high density of kinks would be qualitatively similar.

In units such that $k_B = 1$, the partition function of a string of length l is

$$\mathcal{Z}_1 = (1 + qe^{-\varepsilon_k/T})^{l/l^*} e^{-l\tau/T}, \tag{3.1}$$

where T is the temperature, and q is the two-dimensional coordination number of the lattice on which the defect string lives — for a symmetric vacancy this is the same as that of the original triangular lattice, $q = 6$, whereas for a symmetric interstitial it is that of the dual honeycomb lattice, $q = 3$ (see Sec. VI). The above expression represents the freedom of the string to jump to any of the neighboring lattice sites anywhere along its length. These transverse meanderings cause an entropic lowering of the free energy per unit length of the string:

$$f_1 = \lim_{l\to\infty} -T \ln \mathcal{Z}_1/l = \tau - \frac{T}{l^*}\ln(1 + qe^{-\varepsilon_k/T})$$

$$\simeq \tau - \frac{Tq}{l^*}e^{-\varepsilon_k/T} \quad \text{for} \quad e^{-\varepsilon_k/T} \ll 1. \tag{3.2}$$

If N_k is the total number of kinks, the average kink density is

$$n_k \equiv \frac{\langle N_k \rangle}{l} = \frac{1}{l^*}\frac{qe^{\varepsilon_k/T}}{1 + qe^{\varepsilon_k/T}} \simeq \frac{q}{l^*}e^{-\varepsilon_k/T} \quad \text{for} \quad e^{-\varepsilon_k/T} \ll 1. \tag{3.3}$$

Thus, kinks are on the average $l_k = l^* e^{\varepsilon_k/T}/q$ monomers apart. The assumption of dilute kinks then translates into the condition $l^* n_k \ll 1$, or $\varepsilon_k \gg T$, which can be rephrased as $\langle |\mathbf{u}|^2 \rangle / a_0^2 \ll 1$ [3,4], a condition clearly satisfied by a crystal below its Lindemann melting point.

The above is a ''diffusive'' model for the string—if $\mathbf{d}$ denotes the horizontal end-to-end displacement, the mean square wandering is $\langle |\mathbf{d}|^2 \rangle = 2Dl$, where the ''diffusion constant'' D is given by $2D = a_0^2 n_k$. Consider a continuum description of the string in terms of a function $\mathbf{r}_d(z)$, $\mathbf{r}_d(z)$ being the transverse displacement. Provided the average slope $|d\mathbf{r}_d/dz|$ is small, this ''diffusive'' wandering will correspond to an effective Hamiltonian of the form

$$H_1 = \int_0^l dz \left[\frac{g}{2}\left|\frac{d\mathbf{r}_d}{dz}\right|^2 + \tau \right], \quad g = \frac{T}{D}. \tag{3.4}$$

The continuum approximation to the free energy is appropriate in the limit of large l, since a line subject to kink excitations is always above its roughening transition.

Here we have assumed that the string is wandering within a frozen crystal. However, the lattice around the vacancy or interstitial string responds to its presence by collapsing or expanding around it. For a straight string at $\mathbf{r}_d = \mathbf{0}$, the deformation $\mathbf{u}(\mathbf{r}_\perp, z)$ is given by

$$\mathbf{u}_d(\mathbf{r}_\perp, z) = \pm \frac{\Omega}{2\pi}\frac{\mathbf{r}_\perp}{r_\perp^2} \tag{3.5}$$

in the continuum description of the crystal, that is, away from the defect where the deformations are small. Ω is the area change due to the vacancy or interstitial, $\Omega \simeq a_0^2$. The energy of this deformation has to be included in the energy cost of the defect string. Again invoking the continuum approximation, we assume that for a defect string with small average slope, the resulting deformation away from the string in any plane perpendicular to $\hat{\mathbf{z}}$ will be approximately that resulting from a straight string at the location of the defect in that plane:

$$\mathbf{u}(\mathbf{r}_\perp, z) \simeq \mathbf{u}_d(\mathbf{r}_\perp - \mathbf{r}_d(z), z). \tag{3.6}$$

[In general $\mathbf{u}(\mathbf{r}_\perp, z)$ would depend on the derivatives of $\mathbf{r}_d(z)$ as well.] Within this approximation, the distortion energy of the crystal with bending Frank's constant $K_3 \equiv T l_P \rho$ is, keeping terms up to fourth order in the derivatives (see Appendix A),

$$\frac{\Delta H_1}{T} \sim l_P \int dz \left[\left| \frac{d^2 \mathbf{r}_d}{dz^2} \right|^2, a_0^{-2} \left| \frac{d\mathbf{r}_d}{dz} \right|^4 \right]. \tag{3.7}$$

These impart an effective stiffness to the defect string and suppress transverse fluctuations over a length scale $\sim a_0 \sqrt{DK_3/T} \sim a_0 \sqrt{l_P n_k}$. However, they do not change the long-scale diffusive nature of the string.

The lattice distortions renormalize the diffusion constant of the string when the symmetry direction of the crystal is externally imposed, as in the case of flux lines, or in a polymer crystal with an external field along the $\hat{\mathbf{z}}$ direction. The tilt modulus c_{44} is then nonzero [Eq. (2.4)], and D is renormalized to D_R, where (see Appendix B)

$$\frac{1}{D_R} \simeq \frac{1}{D} + O\left(\frac{c_{44}}{T\rho}\right). \tag{3.8}$$

For a dense vortex *liquid* this effect has been analyzed in detail by Marchetti [15] and D is found to be renormalized to a value independent of its bare value in the long-wavelength limit. The correction comes from convection of a tagged flux line along the local tangent-field direction.

If a similar calculation is carried out for a *crystal* of spontaneously aligned long semiflexible polymers (see Appendix B), one finds a qualitatively different renormalization of D—the correction in the long-wavelength limit is proportional to its bare value, and $\delta D/D \sim 1.45 \langle |\mathbf{u}|^2 \rangle / a_0^2 \lesssim 3\%$ using $c_L^2 \simeq 1/50$ [16] (c_L is the Lindemann constant for melting of a columnar crystal). The correction is negligible. It can be ignored for another reason—the idea of convection of a line by the mean local field, although appropriate for a dense fluid, would not be applicable in a crystalline environment where diffusion can only occur through discrete jumps from column to column. Although thermal fluctuations are already implicit in the exponential factor in $D = a_0^2 n_k/2$ coming from n_k, defects in this case move only on a discrete lattice, without phonon fluctuations.

To summarize this section, we characterize the statistical mechanics of a defect string with a head or tail energy ε_0, a line tension τ, and a diffusion constant D. The latter two can be combined in an effective chemical potential $\overline{\mu} \equiv T\mu_d$ per kink size (l^*) of the string:

$$\mu_d = l^*(-\tau/T + n_k) = q e^{-\varepsilon_k/T} - \varepsilon_k/T, \tag{3.9}$$

with n_k related to D through $D = a_0^2 n_k/2$. Because n_k is exponentially small, $\mu_d \approx -l^*\tau/T \approx -l^* \mu a_0^2/T$ and is usually negative, which suppresses long vacancy and interstitial strings. Turning it positive would require raising the temperature and lowering the kink energy ε_k, and is favored by a larger coordination number q.

Although we have assumed a constant shear modulus, the presence of the defects themselves can drive it down exponentially with the defect concentration, as discussed by Carruzzo and Yu [17]. Thus, positive μ_d becomes possible when softening of the bare elastic constants with increasing defect concentration is taken into account.

IV. STATISTICAL MECHANICS OF NONINTERACTING STRINGS

At any finite temperature, a crystal with a negative string line chemical potential will contain a distribution of thermally excited vacancy and interstitial strings. Since the string energy is proportional to length in the noninteracting-kinks approximation, the equilibrium probability distribution will be an exponentially decaying function of length with mean determined by the line chemical potential, in the dilute string-gas limit where interstring interactions can also be neglected [1]. In discotic crystals string heads and tails can be created as necessary. In a crystal of long polymers, the number of heads and tails is fixed by the mean polymer length.

Let N be the total number of possible kink sites in the lattice, $N = \text{volume} \times \rho/l^*$, and let $\mathcal{P}_l$ be $1/N \times$ the number of defect strings l links long. Assuming that only one kind of defect string is present—those with the lowest line tension—we can write the defect-free energy in terms of $\{\mathcal{P}_l\}$ as [1]

$$\mathcal{F}_d(\{\mathcal{P}_l\}) = \sum_l N\mathcal{P}_l(2\varepsilon_0 - lT\mu_d) + T\sum_l N\mathcal{P}_l(\ln \mathcal{P}_l - 1). \tag{4.1}$$

Minimizing with respect to the $\{\mathcal{P}_l\}$ yields the expected exponential distribution:

$$\mathcal{P}_l = h^2 z^l, \tag{4.2}$$

where $z = e^{\mu_d}$, and the head or tail fugacity $h = e^{-\varepsilon_0/T}$ is expected to be small. For hexagonal columnar crystals of *polymers*, we work in a grand canonical ensemble and adjust ε_0 so that the average head or tail concentration agrees with the fixed value determined by the mean polymer length. The head or tail concentration will be small if the polymers are long. For *discotic* crystals, the grand canonical ensemble is the natural one and the head or tail concentration fluctuates, with an average value determined by the fixed value of $h = e^{-\varepsilon_0/T}$, and the monomer fugacity $z = e^{\mu_d} < 1$. The net defect volume fraction ϕ is

$$\phi \equiv \sum_l l\mathcal{P}_l = h^2 \frac{z}{(1-z)^2}. \tag{4.3}$$

The total number of strings $N_d \equiv N n_s$ is given by the string density

$$n_s \equiv \sum_l \mathcal{P}_l = \frac{h^2}{1-z}. \tag{4.4}$$

A defect monomer is most likely to be found in a string of mean length (in units of the kink size)

$$l_m = \frac{1}{|\mu_d|}. \tag{4.5}$$

The length distribution has an average at $2l_m$, and a spread also of $\sqrt{2}l_m$. The form (4.1) of the energy, linear in l, is really applicable only when $l \gg 1$, so that end effects can be parametrized by the l-independent constant ε_0. Then, μ_d is close to 0, and the relation $\phi \simeq n_s l_{mp}$ holds. The asymptotic behaviors in the dilute and dense limits are as follows:

$$\phi = \begin{cases} h^2 e^{\mu_d}, & z \ll 1 \\ \dfrac{h^2}{|\mu_d|^2}, & z \lesssim 1, \end{cases} \tag{4.6}$$

$$n_s = \begin{cases} h^2, & z \ll 1 \\ \dfrac{h^2}{|\mu_d|}, & z \lesssim 1. \end{cases} \tag{4.7}$$

A string proliferation transition thus occurs at $\mu_d = 0$ in this model, corresponding to a temperature $T_d = \tau l_k$. In the limit $\varepsilon_0 \to \infty$, it corresponds to the appearance of a supersolid phase [2] that is simultaneously crystalline and entangled, where infinitely long vacancy and/or interstitial strings facilitate the wandering and entanglement of lines in the crystalline phase. If the melting temperature $T_m > T_d$, this supersolid or incommensurate solid phase will exist between T_d and T_m.

The noninteracting approximation breaks down in the vicinity of T_d as calculated here, and its estimate will have to be refined by including interactions. For finite ε_0, the sharp transition discussed in Ref. [2] will be blurred, as discussed in Sec. V.

V. ϕ^2 INTERACTION MODEL

Interactions between polymer ends in a columnar crystal have been calculated by Selinger and Bruinsma [13] within the continuum approximation. Because of the uniaxial anisotropy, the interaction has a rather complicated form. The distortion due to an isolated head or tail placed at the origin at in-plane distance $r_\perp$ extends over a vertical extent $|z| \sim \sqrt{\lambda_L r_\perp}$ where $\lambda_L = \sqrt{K_3/c_{11}}$ [see Eq. (2.7)]. The resulting interaction between heads and tails falls as $1/|z|^3$ for predominantly vertical separations z ($|z| \gg \sqrt{\lambda_L r_\perp}$), and as $-1/(\lambda_L r_\perp)^{3/2}$ for predominantly horizontal separations $r_\perp$. In polymer crystals, these contributions must be superimposed on the linear energy cost of the vacancy or interstitial string joining them.

At low defect densities where the string length is much smaller than the average separation of string centers of mass, we have $1/|\mu_d| \ll 1/\phi^{1/3}$, i.e., $|\mu_d| \gg h^{2/3}$, and a string interacts with other strings as a head-tail dipole. The effective interaction between dipoles then falls off very rapidly, becoming short ranged not only in the axial but also in the radial direction.

At the other extreme, the strings are long, which would happen in the vicinity of the head-tail unbinding transition and in the supersolid phase itself. End interactions can then be neglected and the remaining interaction between effectively infinite strings becomes predominantly ''radial'' (i.e., perpendicular to $\hat{\mathbf{z}}$) provided the root mean square tilt with respect to the $\hat{\mathbf{z}}$ axis is small. The defects are then noninteracting in the continuum model unless their anisotropy is taken into account. The interaction between defects with n-fold symmetry ($n = 2$, 3, or 6) falls off at least as fast as $1/r^n$ (see Appendix C). This interaction has an azimuthal dependence of the form $\cos n\theta$ or higher harmonics. The angular average vanishes, leading to an effective interaction that vanishes as an even higher power, which is effectively short-ranged. As mentioned in the Introduction, the lowest-energy vacancy or interstitial defects for simple repulsive pair potentials in the radial direction are in fact of high (threefold or sixfold) symmetry.

We discuss here the simplest model for a short-ranged interaction—a repulsive ϕ^2 model that has been treated earlier in Ref. [3] using a coherent state path integral representation that exploits an analogy with the quantum mechanics of two-dimensional bosons. The defect volume fraction ϕ corresponds to the mean square boson field amplitude $\langle |\psi|^2 \rangle$ in that description. Here, we reproduce the essential results without resorting to the sophisticated boson formalism. Upon adding a term $u\phi^2/2$ to the free energy $f \equiv F/NT$ in Eq. (4.1) of the previous section, we find after minimization,

$$\mathcal{P}_l = h^2 e^{l(\mu_d - u\phi)}. \tag{5.1}$$

As discussed in Ref. [3], the coupling u is an excluded volume parameter describing defect line repulsion. Thus ϕ and N_d have the same form as before, but with z replaced by an effective fugacity ζ:

$$z \to \zeta(z,\phi) \equiv z e^{-u\phi}, \tag{5.2}$$

so that

$$\phi(h,\zeta) = h^2 \frac{\zeta}{(1-\zeta)^2}. \tag{5.3}$$

The volume fraction $\phi(h,z)$ now has to be solved for self-consistently from Eq. (5.3). Note that the effective chemical potential has been reduced by $u\phi$ due to the repulsive interaction:

$$\mu_{eff} \equiv \ln \zeta = \mu_d - u\phi. \tag{5.4}$$

Accordingly, the mean string length l_m changes to

$$l_m = -\frac{1}{\ln \zeta} \equiv \frac{1}{u\phi - \mu_d}. \tag{5.5}$$

The free energy of the distribution is $f \approx -u\phi^2/2$.

The behavior of the string volume fraction for $h = 0$ and $h \neq 0$ is illustrated schematically in Fig. 8. Four distinct regimes emerge, with the following asymptotic behaviors.

(1) For $\mu_d \ll -1$ (point A in Fig. 8),

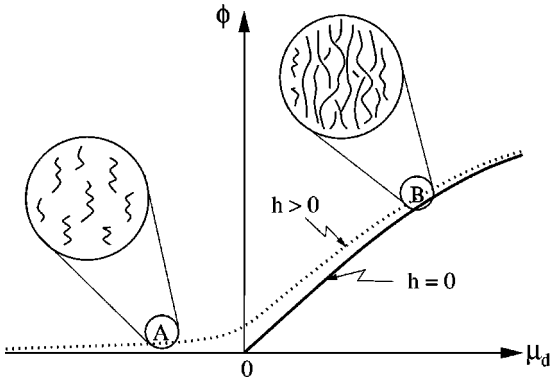

FIG. 8. The volume fraction ϕ is plotted against the effective defect chemical potential μ_d for the ϕ^2 interaction model of a gas of defect strings. The strings are short and dilute in regime A, but long, dense, and entangled in regime B. (Taken from Ref. [3].)

$$\phi \simeq h^2 e^{\mu_d}, \quad n_s \simeq h^2, \quad l_m = \frac{1}{|\mu_d|}. \tag{5.6}$$

This is again the dilute limit where heads and tails are tightly bound.

(2) For $-1 \ll \mu_d \ll -(uh^2)^{1/3}$,

$$\phi \simeq \frac{h^2}{|\mu_d|^2}, \quad n_s \simeq \frac{h^2}{|\mu_d|}, \quad l_m = \frac{1}{|\mu_d|}. \tag{5.7}$$

These results are again identical to those for noninteracting strings. This correspondence is expected, because $|\mu_d| > (uh^2)^{1/3} > u\phi$; therefore the effective chemical potential is still approximately μ_d. The relation $\mu_d \sim -(uh^2)^{1/3}$ marks the limit of validity of the noninteracting approximation, as we argued in the beginning of this section. As we approach this limit, we find for $h \to 0$, $\phi, n_s \to 0$, whereas $l_m \to \infty$. Thus, the strings are still dilute, although lengthening. Note that the results in this regime coincide with those of Ref. [3] in the limit of short and dilute strings.

(3) $|\mu_d| \ll (uh^2)^{1/3} \equiv \mu_c$ (μ_d around the transition which occurs for $h=0$),

$$\phi \simeq \frac{h^2}{|\mu_c|^2}\left[1+\frac{2}{3}\frac{\mu_d}{\mu_c}\right], \quad n_s \simeq \frac{h^2}{|\mu_c|}\left[1+\frac{1}{3}\frac{\mu_d}{\mu_c}\right],$$
$$l_m \simeq \frac{1}{|\mu_c|}\left[1+\frac{1}{3}\frac{\mu_d}{\mu_c}\right]. \tag{5.8}$$

These results can be matched onto those in the noninteracting regime above by replacing μ_d with

$$\mu_{eff} = -\mu_c + \mu_d/3 = -\mu_c\left(1-\frac{\mu_d}{3\mu_c}\right), \tag{5.9}$$

which is now dominated by the repulsive interaction: $\mu_{eff} \approx -u\phi$. The unphysical divergences of the noninteracting model have been suppressed and we find at the transition point

$$\phi = \frac{h^{2/3}}{u^{4/3}}, \quad n_s = \frac{h^{4/3}}{u^{1/3}}, \quad l_m = \frac{1}{u^{1/3}h^{2/3}}. \tag{5.10}$$

Note that all quantities have interesting singularities in the limit $h \to 0$.

If the head or tail fugacity h is small, the defect volume fraction remains negligible at the transition, but the average string length grows large so that it could become greater than the interstring separation, now given by $1/\phi^{1/2}$. Indeed, $1/\phi^{1/2} \ll l_m$ if $h \ll 1/u^2$, which would be true if polymer ends are highly unfavorable.

This long and dilute regime interpolates between the short and dilute and the long and dense limits described in Ref. [3].

(4) For $\mu_d \gg \mu_c$ (point B in Fig. 8), we have

$$\mu_{eff} = -\mu_c\sqrt{\frac{\mu_c}{\mu_d}}. \tag{5.11}$$

The repulsion now keeps in check the string proliferation, and μ_{eff} approaches 0 as $1/\sqrt{\mu_d}$. Thus,

$$\phi \simeq \frac{\mu_d}{u}, \quad n_s \simeq h\sqrt{\frac{\mu_d}{u}}, \quad l_m \simeq \frac{1}{|\mu_c|}\sqrt{\frac{\mu_d}{\mu_c}}. \tag{5.12}$$

This is the phase where strings are dense and entangled—ϕ is $O(1)$. These results also agree with Ref. [3].

As the head or tail fugacity $h \to 0$, the intermediate regime (3) above (around $\mu=0$) shrinks to zero. At $h=0$, heads and tails are completely expelled, and we have a second-order phase transition at $\mu_d=0$ with $\phi=0$ for $\mu_d<0$, and growing as μ_d for $\mu_d>0$, as in Ref. [3]. This limit corresponds to the situation in thermally excited vortex lattices [2] because flux lines cannot start or stop within the sample. In the boson picture, h acts like an external field coupled to the order parameter, injecting magnetic monopoles into the superconductor.

We have neglected vacancy and interstitial loops, which exist even in the limit $h \to 0$. For finite h, their contribution can be neglected near the transition because for long loops, the energy of a loop exceeds the energy of a string of the same vertical extent: Whereas a string of length l has energy $l\tau_{interstitial} + 2\varepsilon_0$ (we expect interstitials to be the preferred defect at the transition in most cases), the energy of a vacancy-interstitial loop of the same length would be approximately l $(\tau_{vacancy} + \tau_{interstitial})$. For large l, the difference $l\tau_{vacancy} - 2\varepsilon_0$ will strongly suppress vacancy and interstitial loops. Because of this energetic barrier, loops cannot become arbitrarily large, and cannot cause entanglement over macroscopic scales. For $h=0$, as is the case for vortex matter, fluctuations in the low-temperature phase are entirely in the form of loops [2], and similar to vortex ring fluctuations in the Meissner phase.

For systems with a finite axial length, the balance may be tilted in favor of long strings because the end penalty is removed if the ends move to the surface and the string threads the sample. For threading strings the expression for entropy in Eq. (4.1) is no longer valid because the freedom in

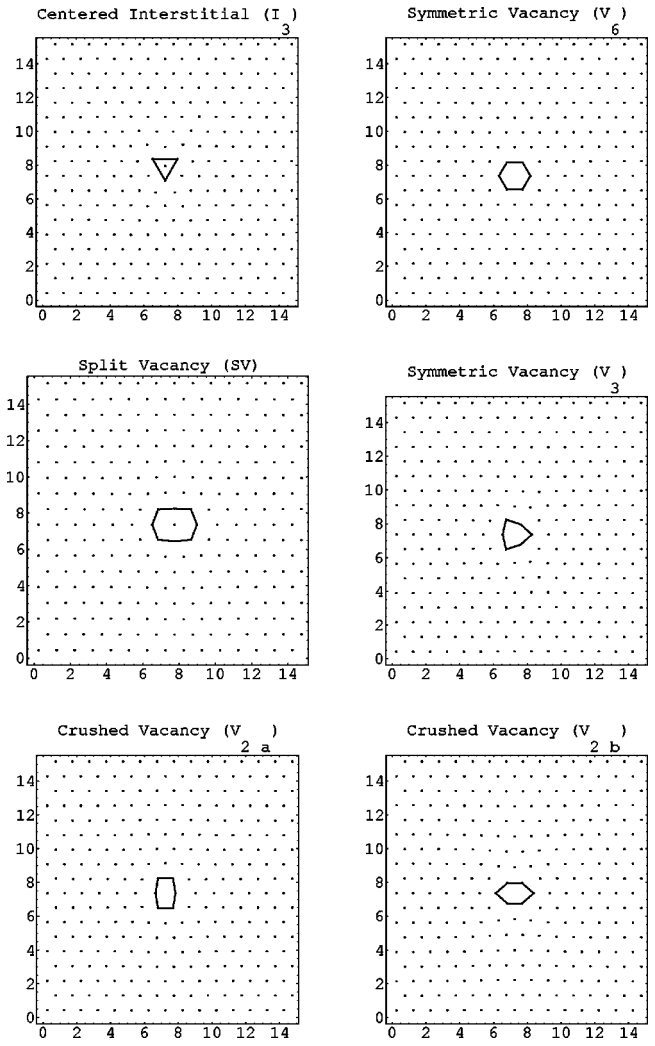

FIG. 9. Various defects obtained in a two-dimensional triangular lattice. The centered interstitial is the only stable interstitial defect.

the z direction is lost. The remaining two-dimensional entropy can be ignored in a three-dimensional system, and we are left with

$$f \simeq -\mu_d \phi + u\phi^2/2, \tag{5.13}$$

where ϕ now is also the areal fraction of defects; and one finds $\phi \simeq \mu_d/u$, similar to region (4) discussed above.

VI. NUMERICAL CALCULATION OF DEFECT LINE TENSIONS

Line tension calculations require that we find the lowest-energy lattice deformation associated with a vacancy or interstitial. These line tensions depend on the *type* of vacancy or interstitial, e.g., whether the defect sits in an environment which is two-, three-, or sixfold symmetric. If thermal fluctuations out of this configuration are small enough to be described within a quadratic approximation, they decouple from the equilibrium configuration. Since these $T=0$ equilibrium defect configurations are composed of straight columns, the three-dimensional deformation energy can be reduced to an effective two-dimensional interaction energy $V(r)$ per unit length between columns separated by distance

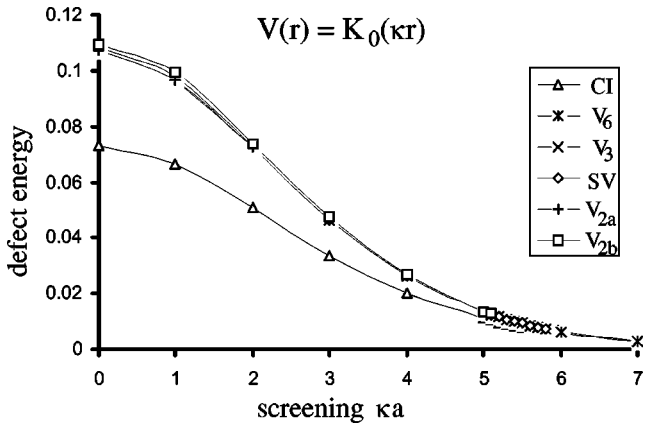

FIG. 10. Defect energy as a function of the screening κa for $V(r)=K_0(\kappa r)$ at system size $n=4$ ($N=480$). Only the centered interstitial is shown, because the edge interstitial is always unstable to it. Various species of vacancies exist, within limited parameter ranges, very close in energy. Lines joining the data points are only an aid to the eye.

r. The calculations can then be performed on a two-dimensional triangular lattice of points interacting with potential $V(r)$. Thus, the defect energies in a two-dimensional Wigner crystal of electrons [18] would correspond to the *line tensions* of the corresponding string defects in a hexagonal columnar crystal of lines interacting with an effective radial $1/r$ potential per unit length.

Such calculations have been carried out by several authors [2,18,19]. Whereas Refs. [18] and [19] have considered defects in a Wigner crystal of electrons ($V_p(r)=1/r$), Frey *et al.* [2] have studied a modified Bessel function potential $V_\kappa(r)=u_0K_0(\kappa r)$ in the $\kappa\to 0$ limit. Here $\kappa \equiv \lambda^{-1}$, where λ is the Debye screening length in the case of long polyelectrolytes in an ionic solution, and the London penetration depth in the case of vortex lines in a type-II superconductor. The limit $\kappa\to 0$ corresponds to a long-range logarithmic interaction, whereas in the short-range limit $\kappa a_0 \gg 1$ the interaction is exponentially decaying. Both Refs. [2] and [19] dealt with long-range interactions ($\ln r$ and $1/r$, respectively), and found that the centered interstitial (see Fig. 9) has the lowest line tension. We denote the centered interstitial by CI, or by I_3 when we want to stress its threefold symmetry. The edge interstitial (denoted EI or I_2) was found to be a saddle point and buckled into a CI. The threefold symmetric centered interstitial CI is the lowest-energy interstitial defect over the entire range of interactions we studied. Among the vacancies, the twofold symmetric crushed vacancy (denoted V_2 or V_{2a} — see Fig. 9) is the only stable one, the symmetric sixfold vacancy (V_6) being unstable to it. The long-range interactions between the energetically preferred types of interstitials and vacancies were found to be attractive for interstitials and repulsive for vacancies.

To determine the correct type of microscopic defect to insert into the phenomenological considerations of Secs. III–V, we have extended the work of Frey *et al.* to the short-ranged regime of the $K_0(\kappa r)$ interaction, to which end we studied values of κa_0 from 0 to 7 (7 being large enough to represent the short-range $\kappa a_0 \to \infty$ limit) (Fig. 10). The aim was to determine the point of crossover from centered interstitials to vacancies as the lowest-energy defect, since it is

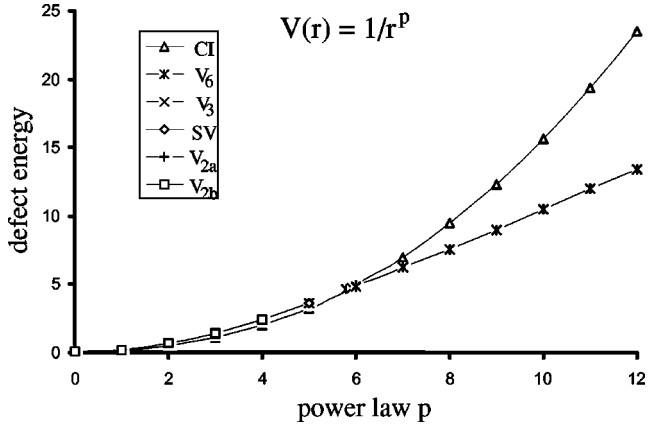

FIG. 11. Defect energy as a function of the power p for $V(r)=1/r^p$ at system size $n=5$ ($N=750$). The apparent increase in energy with p (interaction getting shorter ranged) would go away with proper normalization of the potential. Lines joining the data points are only an aid to the eye.

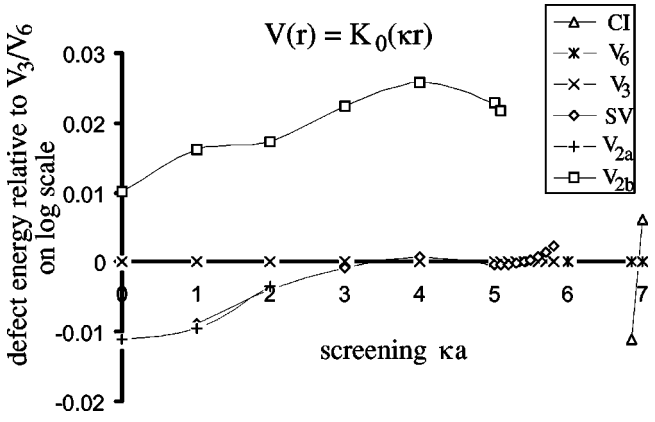

FIG. 12. Defect energies for $V(r)=K_0(\kappa r)$, $n=4$, on the log scale, with respect to V_3 or V_6, in order to illustrate the detailed structure of the energy diagram. The CI can be seen crossing V_6 at $\kappa a \approx 6.9$. Lines joining the data points are only an aid to the eye.

known from simulations of short-range interactions (for a review, see Ref. [20]) that vacancies are preferred in this limit. In the same spirit, we have also extended the Coulomb interaction to power-law interactions $1/r^p$ with exponent values ranging from $p=0$ ($\sim \ln r$) to $p=12$ (Fig. 11).

We checked our minimization procedure by first reproducing the results of Refs. [2] and [19] for $\ln r$ and $1/r$ potentials, respectively. As we move away from the long-range interaction limit $\kappa a=0$, the metastable crushed vacancy (V_{2a}) exchanges stability with the metastable split vacancy (SV), also of twofold symmetry. Two metastable species, a threefold symmetric vacancy (V_3) and a two-fold symmetric vacancy (V_{2b}) crushed along the basis vector of a triangular unit cell, also exist, but are of higher energy. The differences in energy can be as small as one part in a few thousand. As the interaction gets shorter ranged, V_{2b} loses stability to V_3 at $\kappa a_0 \simeq 5.2$, and the threefold deformation of V_3 gets smaller so that it transforms continuously into V_6 at $\kappa a_0 \simeq 5.9$. When V_6 appears, the SV also loses stability to it. By the time I_3 and V_6 finally cross in energy, V_6 is the only stable vacancy left. The crossing happens at surprisingly large parameter values, $\kappa a_0 \simeq 6.9$ for $V_{\kappa a}$ (Fig. 12), and $p \simeq 5.9$ for V_p (Fig. 13), each very close to the short-range limit. We thus find that the interstitial has a very wide range of stability, extending well into the short-ranged regime.

Following previous authors, the simulations were performed in an almost square (length-to-width ratio $5:3\sqrt{3}$) cell containing $N=5n\times 6n=30n^2$ lattice points with $n=1-5$ [rather than a more nearly square but bigger rectangle of, say, $7n\times 8n$ ($7:4\sqrt{3}$), which would allow us to sample a smaller number of system sizes n with a given computational limit on N]. Figure 9 corresponds to $n=3$.

A defect is introduced by adding or removing a particle, and then allowing the resulting configuration to relax. The difference between the energies of the relaxed defect configuration and the perfect lattice configuration gives the energy of the defect. There are two modifications to this simple calculation. We want the defect energy corresponding to the physical conditions of constant chemical potential or line density, so we rescale the cell dimensions (by changing the lattice constant a_0) after inserting the defect to restore the system to its original density (following Ref. [19]). Moreover, since we would ideally like to study an infinite system, the large but finite cell containing $30n^2$ particles is assumed to be repeated in all directions, so that we are effectively dealing with a periodic array of defects, or an infinite lattice in the absence of a defect. The periodic boundary conditions maintain the average line density during the relaxation process. However, now the energy per cell also includes the energy of interaction of a defect with all its periodic images. As discussed earlier, this energy is finite, and by extrapolating its dependence on cell size n, i.e., interdefect separation ($\approx 5n$), to large n, the energy of an isolated defect can be extracted [2,19].

For short-ranged interactions, the energy calculation can be simplified. We introduce a cutoff interaction radius r_c where the interaction falls to a small fraction of its nearest-neighbor value. The interaction with the particles outside can be approximately accounted for by assuming a uniform density outside and integrating over it. The radius r_c is chosen to make this correction small compared to the total energy, say, less than 10^{-3} of it. Interactions within the shell are calculated explicitly. As long as $r_c < L/2$, L being the cell width, this short-range method should be very accurate.

For long-ranged interactions such as $\ln r$, $1/r$, or $1/r^2$, the

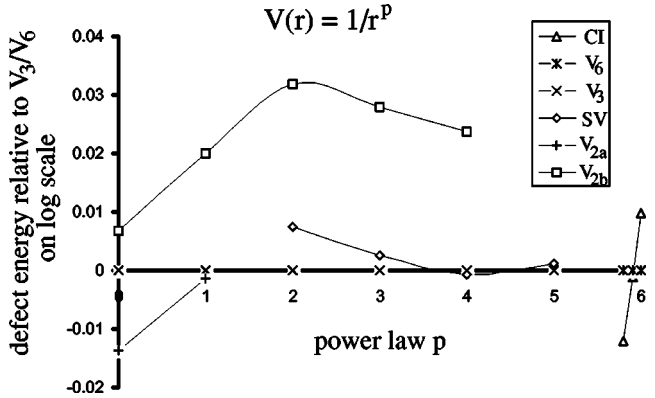

FIG. 13. Defect energies for $V(r)=1/r^p$, $n=5$, on the log scale, with respect to V_3 or V_6. The CI and V_6 cross at $p \approx 5.9$. Lines joining the data points are only an aid to the eye.

TABLE I. Defect energies for $V(r)=K_0(\kappa r)$; $a_0=1$; system size $n=4$ ($N=480$). The upper part corresponds to the Ewald sum method for long-range interactions, the lower part to a simple cutoff method for short-range interactions. The centered interstitial and the symmetric vacancy cross at $\kappa a \approx 6.9$. Entries such as ''V_{2a},'' ''SV,'' ''V_3,'' and ''V_6'' indicate an instability to a lower-energy defect.

κa	I_3	SV	V_{2a}	V_3	V_{2b}	V_6
0	0.073016802	V_{2a}	0.107018876	0.108206944	0.109320135	V_3
1	0.066331581	0.096728537	0.096661116	0.097578530	0.099169907	V_3
2	0.050588818	0.072306827	0.072341149	0.072594220	0.073852944	V_3
3	0.033575192	0.046095915	SV	0.046131759	0.047174061	V_3
4	0.020037313	0.025980648	SV	0.025962421	0.026641900	V_3
4	0.020036	0.025980	SV	0.025961	0.026641	V_3
5	0.0110170	0.0133112	SV	0.0133146	0.0136217	V_3
5.1	0.010338333	0.012397139	SV	0.012400742	0.012674362	V_3
5.2	0.009695442	0.011537972	SV	0.011541059	V_3	V_3
5.3	0.009087036	0.010731274	SV	0.010733113	V_3	V_3
5.4	0.008511788	0.009974612	SV	0.009974441	V_3	V_3
5.5	0.007968369	0.009265581	SV	0.009262603	V_3	V_3
5.6	0.007455456	0.008601808	SV	0.008595187	V_3	V_3
5.7	0.006971737	0.007980968	SV	0.007969812	V_3	V_3
5.8	0.006515917	0.007400791	V_3	0.007384121	V_3	V_3
5.9	0.006086722	V_6	V_6	V_6	V_6	0.006835768
6	0.005682901	V_6	V_6	V_6	V_6	0.006322377
7	0.002788486	V_6	V_6	V_6	V_6	0.002771295

above method breaks down, and we must resort to the Ewald summation technique [21,22], which yields an effective two-particle interaction that includes the interaction of one particle with all the periodic images of the other. This effective potential consists of a real space sum (corresponding to a screened interaction) and a reciprocal space sum (corresponding to the screening charge). The division between the two is controlled by an Ewald parameter, and by a judicious choice of its value, the interaction can be made sufficiently short ranged for both sums. We then employ cutoffs in both spaces, with values determined by the desired precision (see Appendix C for details).

To find the minimum of the interaction energy as a function of the configuration of N particles, we use the conjugate-gradient method [23]. The forces are also needed for this method, and are easily derived from the energy and conveniently calculated along with it.

The results for $n=4$ (480 particles) for $V_{\kappa a}$ and for $n=5$ for V_p (750 particles) are shown in Tables and I and II and Figs. 10 and 11. ($n=5$ was computationally prohibitive

TABLE II. Defect energies for $V(r)=1/r^p$; $a_0=1$; system size $n=5$ ($N=750$). The Ewald sum technique was used to calculate the energies. The centered interstitial and the symmetric vacancy cross at $p \approx 5.9$. Entries such as ''V_3'' and ''V_6'' indicate an instability to a lower energy defect.

p	I_3	SV	V_{2a}	V_3	V_{2b}	V_6
0	0.073061685	V_{2a}	0.106775085	0.108253779	0.108994418	V_3
1	0.146421440	V_{2a}	0.209046876	0.209331872	0.213568209	V_3
2	0.487928019	0.677444176	SV	0.672359275	0.694143882	V_3
3	1.08543992	1.39071722	SV	1.38704618	1.42628053	V_3
4	1.99663790	2.37494467	SV	2.37649196	2.43341170	V_3
5	3.2620983	3.5889518	SV	3.5851010	V_3	V_3
5.8	4.5498400	V_6	V_6	V_6	V_6	4.6053332
5.9	4.7286554	V_6	V_6	V_6	V_6	4.7341340
6	4.9114956	V_6	V_6	V_6	V_6	4.8637723
7	6.9642383	V_6	V_6	V_6	V_6	6.1999848
8	9.4317462	V_6	V_6	V_6	V_6	7.5920876
9	12.319586	V_6	V_6	V_6	V_6	9.0220754
10	15.629229	V_6	V_6	V_6	V_6	10.477581
11	19.359421	V_6	V_6	V_6	V_6	11.950259
12	23.495660	V_6	V_6	V_6	V_6	13.434556

for the long-ranged regime with $\kappa a_0 > 0$). Note that, for the screened Bessel function interaction, we find that calculations optimized for the long- and short-ranged regimes agree to within 1 part in 20 000 at $\kappa a_0 = 4$. Moreover, we find that the interaction of a defect with all its periodic images is repulsive for defects with (even) two- and sixfold symmetry, and attractive for (odd) threefold symmetry, consistent with Ref. [2]. As discussed in Refs. [2] and [19], the true asymptotic form of the power-law defect interaction probably is not reached for the distance scales $r \sim 20-30$ lattice spacings studied here.

VII. CONCLUSIONS

We have studied factors contributing to the wandering of a vacancy or interstitial string defect in a hexagonal columnar crystal. A gas of such strings in the crystalline phase, interacting via short-range potentials, can proliferate via continuous or first-order transitions when the corresponding defect chemical potential changes sign, leading to a supersolid phase. The transition can be modified by the presence of vacancy or interstitial loops, especially in a system of finite thickness. We have also numerically calculated defect line tensions for two families of line interactions which interpolate between long- and short-ranged interaction potentials. In each case, we determine the point where interstitial and vacancy defects exchange stability. A complete accounting requires consideration of a variety of nearly degenerate vacancy configurations. At finite temperatures, the small energy differences between different species will further lower the free energy of the vacancy through a gain in fluctuation entropy. The interstitial itself can fluctuate between the centered and edge configurations. The point where vacancies and interstitials exchange stability will shift at finite temperatures due to entropic effects of this kind. In the context of long-range potential calculations, we show in Appendix D how to extend the Ewald summation to the modified Bessel function potential $K_0(x)$.

ACKNOWLEDGMENTS

This research was supported by the National Science Foundation, in part by the MRSEC Program through Grant No. DMR-9400396 and through Grant No. DMR-9714725.

APPENDIX A: CALCULATION OF ENERGY OF DISTORTION DUE TO A DEFECT STRING

As described in Ref. [13], minimization of the free energy (2.1) with the constraint (2.6) yields the following equation for $\mathbf{u}(\mathbf{r}_\perp, z)$:

$$\lambda_L^2 \partial_z^4 \mathbf{u} - \boldsymbol{\nabla}_\perp (\boldsymbol{\nabla}_\perp \cdot \mathbf{u}) = \frac{1}{\rho_0} \boldsymbol{\nabla}_\perp \delta(\mathbf{r}_\perp - \mathbf{r}_d), \tag{A1}$$

$\mathbf{r}_d$ being the in-plane location of the defect string (assumed straight for now). Upon assuming a solution of the form $\mathbf{u} = -(1/\rho_0)\boldsymbol{\nabla}_\perp \psi$, we have the scalar equation

$$(-\lambda_L^2 \partial_z^4 + \nabla_\perp^2)\psi = \delta(\mathbf{r}_\perp - \mathbf{r}_d). \tag{A2}$$

For the straight string, the solution is

$$\psi(\mathbf{r}_\perp, z) \propto \ln|\mathbf{r}_\perp - \mathbf{r}_d|, \quad \text{or} \quad \mathbf{u}(\mathbf{r}_\perp, z) \propto \frac{\mathbf{r}_\perp - \mathbf{r}_d}{|\mathbf{r}_\perp - \mathbf{r}_d|^2}, \tag{A3}$$

with proportionality constant $\sim a_0^2$.

Now consider a wandering string with a dilute concentration of kinks, described on average by $\mathbf{r}_d(z)$ (see Fig. 1). Upon inserting this z dependence into the right hand side (RHS) of Eq. (A2), we see that the resulting ψ inherits the fluctuations of $\mathbf{r}_d(z)$. If l_z represents the smallest wavelength in $\mathbf{r}_d(z)$, the two terms on the LHS of Eq. (A2) compare as λ_L^2/l_z^4 vs $1/a_0^2$, or as l^* vs l_z where $l^* = \sqrt{\lambda_L a_0}$ is of the order of the kink length. Since the meandering of the defect string occurs on a length scale much larger than the kink size, the first term should be negligible compared to the second, and we can set

$$\psi(\mathbf{r}_\perp, z) \propto \ln|\mathbf{r}_\perp - \mathbf{r}_d(z)| \tag{A4}$$

as a reasonable approximation.

The elastic energy of a defect of length L can now be written as

$$E_{defect} = \tau_z L + \varepsilon_k \int \frac{dz}{a_0} \left| \frac{d\mathbf{r}_d(z)}{dz} \right| + \frac{1}{2} \int' d^3r \, K_3 \left(\frac{\partial^2 \mathbf{u}}{\partial z^2} \right)^2, \tag{A5}$$

representing contributions from line tension, kinks, and the bending energy of the distorted crystal (zero for a straight string). The primed integral here excludes the core of the string: a region of radius $\sim a_0$ around it. It can easily be evaluated for $\mathbf{u}(\mathbf{r}, z) = \mathbf{u}_d(\mathbf{r}_\perp - \mathbf{r}_d(z), z)$ and reduces to the form in Eq. (3.7), accurate up to fourth order in the derivatives. The second term, on the other hand, leads to the term $(g/2)\int dz |d\mathbf{r}_d/dz|^2$ in Eq. (3.4). For long wavelengths, the additional contribution from the third term is irrelevant in comparison, being of higher order in the derivatives. The length scale at which it becomes important is obtained by balancing the two terms: $K_3/l_z^4 \sim T/D/l_z^2$, or $l_z \sim \sqrt{K_3 D/T}$.

APPENDIX B: RENORMALIZATION OF *D* BY DEFECT-PHONON COUPLING

In Sec. III we described the wandering of a defect line along the $\hat{\mathbf{z}}$ axis by a ''diffusion'' constant $D = a_0^2 n_k/2$, corresponding to an effective Hamiltonian [Eq. (3.4)] $H_{defect} = (g/2)\int dz |d\mathbf{r}_d/dz|^2$, $\mathbf{r}_d(z)$ describing the in-plane position of the defect string, with $g = T/D$. To incorporate the effect of lattice fluctuations on the diffusion of the defect string, we modify H_{defect} to

$$H_{defect\text{-}phonon} = \frac{g}{2} \int dz \left| \pm \frac{d\mathbf{r}_d}{dz} + \mathbf{t}(\mathbf{r}_d, z) \right|^2, \tag{B1}$$

where the expression in brackets now represents the deviation of the vacancy or interstitial string with respect to the local director

$$\mathbf{t} \equiv \frac{\partial \mathbf{u}}{\partial z}. \tag{B2}$$

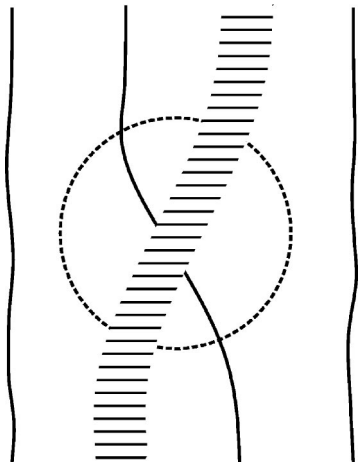

FIG. 14. Illustration of the coupling between a defect string and the lattice distortion. In this case, the change in the position of the vacancy string (thick dashed curve) is equal and opposite to the change in the phonon displacement field.

Figure 14 illustrates the case of a vacancy string, which we shall assume for the remainder of this appendix.

It is easy to derive the diffusion equation for the partition function $\mathcal{Z}(\mathbf{r}_d,\mathbf{r}_0;z,0)$ corresponding to the above Hamiltonian [the $\{\mathbf{u}(\mathbf{r}_\perp,z)\}$ dependence in $\mathcal{Z}$ has been omitted for convenience]:

$$\partial_z\mathcal{Z}-(\mathbf{t}\cdot\boldsymbol{\nabla}_\perp)\mathcal{Z}=D\nabla_\perp^2\mathcal{Z}. \tag{B3}$$

$\mathcal{Z}$ represents the probability density for the defect position; $-\mathbf{t}$ is the ''convective velocity'' for this density. It can also be thought of as an (imaginary) vector potential acting on a particle of mass g in two dimensions, with z the timelike coordinate.

Defining the propagator $G(\mathbf{r}_\perp,z)=\mathcal{Z}(\mathbf{r}_\perp,z)\theta(z)$, $\theta(z)$ being the step function, G obeys

$$(\partial_z-D\nabla_\perp^2)G(\mathbf{r}_\perp,z)=\delta^{(2)}(\mathbf{r}_\perp)\delta(z)+\mathbf{t}\cdot\boldsymbol{\nabla}_\perp G. \tag{B4}$$

The bare propagator G_0 corresponds to ignoring the convective influence of the medium. Thus, G_0 satisfies

$$(\partial_z-D\nabla_\perp^2)G_0(\mathbf{r}_\perp,z)=\delta^{(3)}(\mathbf{r}). \tag{B5}$$

Fourier-transforming $\mathbf{r}_\perp\to\mathbf{k}$ (spacelike) and $z\to\omega$ (timelike),

$$G_0(\mathbf{k},\omega)=(-i\omega+D\mathbf{k}^2)^{-1}. \tag{B6}$$

The renormalized diffusion coefficient D_R will be calculated from the average of G over the phonon degrees of freedom using the definition

$$G(\mathbf{k},\omega)^{-1}=-i\omega+D_Rk^2 \tag{B7}$$

in the limit $|\mathbf{k}|,\omega\to0$. Upon denoting $k\equiv(\mathbf{k},\omega)$, Eq. (B4) becomes

$$G_0^{-1}(k)G(k)=1+\int_{k'}i\mathbf{k}'\cdot\mathbf{t}(k-k')G(k'). \tag{B8}$$

The symbol $\int_k$ denotes $\int d^3k/(2\pi)^3$. Equation (B8) can be expanded in a perturbation series:

$$\begin{aligned}G(k)=G_0(k)&+G_0(k)\int_{k'}i\mathbf{k}'\cdot\mathbf{t}(k-k')G_0(k')\\&+G_0(k)\int_{k'}i\mathbf{k}'\cdot\mathbf{t}(k-k')G_0(k')\\&\times\int_{k''}i\mathbf{k}''\cdot\mathbf{t}(k'-k'')G_0(k'')+\cdots.\end{aligned} \tag{B9}$$

To calculate the thermal averages of products of $\mathbf{t}=-i\omega\mathbf{u}$, we need

$$\langle u_\alpha(k)\rangle=0,$$

$$\langle u_\alpha(k)u_\beta(k')\rangle=[S_L(k)\mathcal{P}^L_{\alpha\beta}(k)+S_T(k)\mathcal{P}^T_{\alpha\beta}(k)]\delta^{(3)}(k-k') \tag{B10}$$

$$\equiv S_{\alpha\beta}(k)\delta^{(3)}(k-k'), \tag{B11}$$

where the correlation functions parallel (L) and perpendicular (T) to $\mathbf{k}$ are

$$S_{L/T}(k)=\frac{T}{K_3\omega^2+c_{11/66}k^2} \tag{B12}$$

and the projection operators are $\mathcal{P}^L_{\alpha\beta}(k)=k_\alpha k_\beta/k^2$ and $\mathcal{P}^T_{\alpha\beta}(k)=\delta_{\alpha\beta}-\mathcal{P}^L_{\alpha\beta}(k)$. Therefore

$$\begin{aligned}\langle G(k)\rangle=G_0(k)-G_0(k)\Bigg[&\int_{k'}k_\alpha k'_\beta\omega^2S_{\alpha\beta}(k-k')\\&\times G_0(k')\Bigg]G_0(k)+\cdots.\end{aligned} \tag{B13}$$

Diagrammatically, this series is represented in Fig. 15. All diagrams of type (b) and (c) reducible to the one-loop diagram (b) can be summed to give $\langle G(k)\rangle^{-1}\approx G_0(k)^{-1}+V(k)$ where $V(k)$ is the term in square brackets in Eq. (B13). Then, $D_R=D+\delta D_R$ where

$$\delta D_R\approx\lim_{k\to0}\frac{1}{2}\nabla_{\mathbf{k}}^2V(k). \tag{B14}$$

With the assumption $\lambda_{L/T}D^2a_0^{-3}\ll1$, in other words, kink size $l^*\ll l_k$, the kink separation δD_R can be evaluated to give

$$\frac{\delta D_R}{D}\approx\frac{T}{K_3^{1/4}}\left(\frac{1}{c_{11}^{3/4}}+\frac{1}{c_{66}^{3/4}}\right)\frac{\Lambda^{5/2}}{20\sqrt{2}\pi}, \tag{B15}$$

where we have imposed a cutoff by replacing the hexagonal Brillouin zone by a circle of radius $\Lambda\equiv4\pi/\sqrt{3}a_0$ which has the same area. If $c_{66}\ll c_{11}$, the fluctuations are mostly transverse, and

$$\frac{\delta D_R}{D}\approx\frac{\langle|\mathbf{u}|^2\rangle}{a_0^2}\frac{4\pi}{5\sqrt{3}}. \tag{B16}$$

Since $\langle|\mathbf{u}|^2\rangle/a_0^2\lesssim c_L^2$, where the Lindemann ratio for hexagonal columnar crystalline lattices is empirically known to be $c_L^2\simeq1/50$ [16], we find $\delta D_R/D<3\%$.

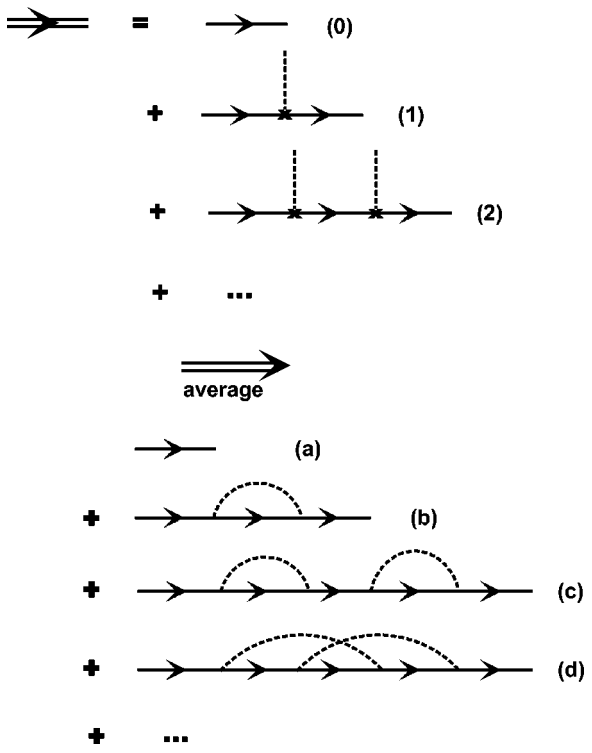

FIG. 15. Diagrammatic representation of the series expansion of the propagator for the defect probability density. The average is over the phonon degrees of freedom.

APPENDIX C: INTERACTION BETWEEN DEFECTS WITH *n*-FOLD SYMMETRY

We assume the defect string to be straight, so that only the planar elastic deformation energy $\mathcal{F}_{crystal}$ (Eq. 2.3) is relevant. In the continuum model discussed, this energy is isotropic in the strains u_{ij}. The stress $\sigma_{ij}=\delta\mathcal{F}_{crystal}/\delta u_{ij}$ can be expressed in terms of a biharmonic stress function χ [24], $\nabla_\perp^2\nabla_\perp^2\chi=0$, as $\sigma_{ij}=\epsilon_{ik}\epsilon_{jl}\partial_k\partial_l\chi$ (ϵ_{ij} is the two-dimensional antisymmetric tensor, $\epsilon_{12}=1$).

For a dislocation with Burgers vector $\mathbf{b}$, $\chi=-K\hat{z}\cdot(b\times r_\perp)\ln r_\perp$, where $K=\mu(\lambda+\mu)/\pi(\lambda+2\mu)$ in terms of the Lamé coefficients.

We construct χ for an n-fold symmetric vacancy or interstitial by treating it as a superposition of n dislocations (bound) symmetrically placed a distance $d\approx a_0$ apart (such that the volume of the defect is $\Omega\sim nda_0$), with Burger vectors separated by $2\pi/n$ in orientation. The resulting stress function has a form satisfying

$$\nabla_\perp^2\chi=K\Omega\left(2\pi\delta^{(2)}(\mathbf{r}_\perp)-\frac{1}{d^2}\sum_{k=1}^{\infty}a_k\frac{\cos kn\theta}{(r_\perp/d)^{kn}}\right) \quad \text{(C1)}$$

where a_k are coefficients of $O(1)$.

The interaction energy of two such defects, located at $\mathbf{r}_1$ and $\mathbf{r}_2$, respectively, can be written in terms of their stress functions as

$$\mathcal{U}_{12}(\mathbf{r}_{12}\equiv\mathbf{r}_2-\mathbf{r}_1)=\frac{1}{4\pi K}\int d^2r_\perp\nabla_\perp^2\chi(\mathbf{r}_\perp-\mathbf{r}_1)\nabla_\perp^2\chi(\mathbf{r}_\perp-\mathbf{r}_2). \quad \text{(C2)}$$

For $r_{12}/d\gg1$, the leading term in the interaction comes from the convolution of the δ function with the $k=1$ term (in other words, this is the cost of the volume change produced by one defect in the stress field of the other); therefore it is of the form $\cos n\theta_{12}/r_{12}{}^n$.

Specifically, we find for vacancies (the sign is reversed for interstitials)

n	Relative orientation	$\mathcal{U}(\mathbf{r}_\perp)$ (units of $K\Omega/d^2$)
2	parallel	$\dfrac{-\cos 2\theta+\cos 4\theta}{(r/d)^2}$
2	perpendicular	$\dfrac{-2\cos 2\theta+\cos 4\theta}{(r/d)^2}$
3	parallel	$\dfrac{-3\cos 6\theta}{(r/d)^4}$
3	antiparallel	$\dfrac{-2\cos 3\theta}{(r/d)^3}+\dfrac{3\cos 6\theta}{(r/d)^4}$
6		$\dfrac{-2\cos 6\theta}{(r/d)^6}$

APPENDIX D: EWALD SUM FOR $V(R)=K_0(\kappa R)$ AND $1/R^p$

Let $\phi(r)$ be the two-body interaction potential between charges q_i in the given system so that the total interaction energy is

$$U=\frac{1}{2}\sum_{i\neq j}\sum q_iq_j\phi(r_{ij}). \quad \text{(D1)}$$

The simulated system consists of N particles in a cell repeated to generate an infinite system. Then the energy per cell can be written as

$$U=U_{0_\alpha}+\frac{1}{2}\sum_{i\neq j}^{N}\sum q_iq_jv_\alpha(r_{ij}), \quad \text{(D2)}$$

where [21]

$$v_\alpha(r_{ij})=\sum_{\mathbf{n}}[\phi(\mathbf{r}_{ij}+\mathbf{n})-\psi_\alpha(\mathbf{r}_{ij}+\mathbf{n})]+\frac{1}{A}\sum_{\mathbf{G}}\tilde{\psi}_\alpha(\mathbf{G})e^{i\mathbf{G}\cdot\mathbf{r}_{ij}}, \quad \text{(D3a)}$$

$$U_{0_\alpha}=\frac{1}{2}\left(\sum_i q_i^2\right)\lim_{\mathbf{r}\to0}[v_\alpha(\mathbf{r})-\phi(\mathbf{r})]. \quad \text{(D3b)}$$

Here the sum over $\mathbf{n}$ consists of all real space lattice vectors of the lattice generated by a cell of area A, and the sum over $\mathbf{G}$ goes over the corresponding reciprocal lattice vectors. The lattice is rectangular (almost square) in our case, which makes it easy to list these vectors. ψ_α is the long-range part of the interaction ϕ, so that $\phi-\psi_\alpha$ is a screened, short-ranged interaction. $\tilde{\psi}_\alpha$ is the Fourier transform. The amount

of screening is controlled by the Ewald parameter α. If we take α to be large enough so that the real space sum can be truncated at $r_c = L/2$ within the desired precision, then we can drop the sum over $\mathbf{n} \neq \mathbf{0}$ [25]. However, this means including more short-range components in the screening charge distribution, so that it spreads to higher reciprocal vectors. The cutoff in reciprocal space is again determined by the precision required.

Since we shall be considering N particles, each with $q_i = 1$, we have $\Sigma_i q_i^2 = N$ and $(\Sigma_i q_i)^2 = N^2$. Rearranging the sums in U and noting that $N/A \equiv \rho$, which is constant throughout the calculation, we can rewrite U as

$$U = U_{ref} + U_{int}, \tag{D4}$$

where [21,25]

$$U_{int} \approx \sum_{i<j}^{N} \sum [\phi(\mathbf{r}_{ij}) - \psi_\alpha(\mathbf{r}_{ij})] + \frac{1}{2A} \sum_{\mathbf{G}} \tilde{\psi}_\alpha(\mathbf{G}) \times \left[\left(\sum_i \cos \mathbf{G}\cdot\mathbf{r}_i \right)^2 + \left(\sum_i \sin \mathbf{G}\cdot\mathbf{r}_i \right)^2 \right], \tag{D5a}$$

$$U_{ref} \approx -\frac{N}{2} \lim_{\mathbf{r}\to 0} \psi_\alpha(\mathbf{r}) + \frac{N}{2} \rho \lim_{\mathbf{k}\to 0} \tilde{\psi}_\alpha(\mathbf{k}). \tag{D5b}$$

Note that U_{ref} is explicitly proportional to N in this form. This is the form we use in our calculations. For interactions whose long-range integral diverges (such as $1/r^p$ with $p \leqslant 2$), a uniformly spread background of equal and opposite charge is assumed, so that the second term in U_{ref} should contain

$$\lim_{\mathbf{k}\to \mathbf{0}} [\tilde{\psi}_\alpha(\mathbf{k}) - \tilde{\phi}(\mathbf{k})]. \tag{D6}$$

We can now proceed to the special potentials we are interested in. For the power-law potential

$$\phi(r) = 1/r^p \equiv \frac{1}{\Gamma(p/2)} \int_0^\infty dt\, t^{p/2-1} e^{-tr^2}, \tag{D7}$$

we take [26]

$$\psi_\alpha(r) = \frac{1}{\Gamma(p/2)} \int_{\alpha^2}^\infty dt\, t^{p/2-1} e^{-tr^2} \equiv \frac{1}{r^p} \frac{\Gamma(p/2, (\alpha r)^2)}{\Gamma(p/2)}, \tag{D8}$$

so that the screened interaction is

$$\phi(r) - \psi_\alpha(r) = \frac{1}{r^p} \frac{\gamma(p/2, (\alpha r)^2)}{\Gamma(p/2)}. \tag{D9}$$

(Γ and γ are complementary incomplete Gamma functions [27].)

The Fourier transform is ($d = 2$)

$$\tilde{\psi}_\alpha(k) = \frac{\pi^{d/2}}{\Gamma(p/2)} \left(\frac{2}{k} \right)^{d-p} \Gamma\left[\frac{d-p}{2}, \left(\frac{k}{2\alpha} \right)^2 \right]. \tag{D10}$$

Also,

$$\lim_{r\to 0} \psi_\alpha(r) = \frac{\alpha^p}{\Gamma(p/2+1)}, \tag{D11}$$

$$\lim_{k\to 0} \tilde{\psi}_\alpha(k) = \frac{2}{p-d} \frac{\pi^{d/2} \alpha^{p-d}}{\Gamma(p/2)}, \quad p > d. \tag{D12}$$

For $p < d$, the above expression corresponds to $\lim_{k\to 0} [\tilde{\psi}_\alpha(k) - \tilde{\phi}(k)]$. For $p = d$, both forms would diverge; however, they would be independent of α, and since the defect energy is a difference of energies, this term would cancel out.

The force on particle j, $\mathbf{f}_j \equiv -\nabla_j U$, can also be written as a sum of real space and reciprocal space contributions:

$$\mathbf{f}_j = \sum_{i\neq j} \mathbf{f}_{ij}^R + \mathbf{f}_j^G, \tag{D13a}$$

where

$$\mathbf{f}_{ij}^R = 2 \frac{\Gamma(p/2+1, (\alpha r_{ij})^2)}{r_{ij}^{p+2}} \mathbf{r}_{ij} \tag{D13b}$$

is the sum of forces on particle j due to particle i and all its images, and

$$\mathbf{f}_j^G = \frac{1}{A} \sum_{\mathbf{G}\neq \mathbf{0}} \tilde{\psi}_\alpha(G) \left[\left(\sum_i \cos \mathbf{G}\cdot\mathbf{r}_i \right) \sin \mathbf{G}\cdot\mathbf{r}_j - \left(\sum_i \sin \mathbf{G}\cdot\mathbf{r}_i \right) \cos \mathbf{G}\cdot\mathbf{r}_j \right] \mathbf{G} \tag{D13c}$$

is the sum of forces on particle j due to all images of itself.

The coordinates $\mathbf{r}$ here are normalized such that $a_0 = 1$. When we change N to $N_d = N \pm 1$ and rescale a_0 to $a = \sqrt{N_d/N}$ after inserting a defect, we chose to keep $\mathbf{r}$ normalized with respect to a, so that it picks up a factor of a. If we also scale α by $1/a$, the product αr remains unchanged (as does $\mathbf{G}\cdot\mathbf{r}$), so that we can keep using the original values of α and $\mathbf{G}$ in U_{int} and $\mathbf{f}$, and scale the result by $1/a^p$ in the end. In U_{ref} we have to use the scaled value of α along with N_d, and subtract the energy of the perfect lattice scaled by N_d/N.

On the other hand, if we do not scale α, U_{ref} cancels out, but α has to be replaced by αa in U_{int} and $\mathbf{f}$.

For the modified Bessel function interaction

$$\phi(r) = K_0(\kappa r) \tag{D14}$$

(where κ represents κa because of the normalization of r), the $\kappa = 0$ case, corresponding to $\phi(r) \sim -\ln r$, has been treated by Frey *et al.* [2]. To extend this to $\kappa > 0$, we perform an expansion similar to that of Silva and Mokross [28] for a Yukawa potential. Writing the potential in integral form,

$$\phi(r) = K_0(\kappa r) \equiv \frac{1}{2} \int_0^\infty \frac{dt}{t} e^{-t} e^{-(\kappa r)^2/4t}, \tag{D15}$$

we choose the screened interaction to be

$$\phi(r)-\psi_\alpha(r)=\frac{1}{2}\int_{(\alpha r)^2}^{\infty}\frac{dt}{t}e^{-t}e^{-(\kappa r)^2/4t}$$
$$=\frac{1}{2}\int_1^{\infty}\frac{ds}{s}e^{-(\alpha r)^2 s}e^{-(\kappa/2\alpha)^2(1/s)}. \quad \text{(D16)}$$

Expanding the exponential within the integral in a Taylor series about $\kappa=0$, we get

$$\phi(r)-\psi_\alpha(r)=\frac{1}{2}\sum_{n=0}^{\infty}\frac{(-1)^n}{n!}\left(\frac{\kappa}{2\alpha}\right)^{2n}E_{n+1}((\alpha r)^2), \quad \text{(D17)}$$

where $E_n(x)$ is the exponential integral function $[E_{n+1}(x)=x^n\Gamma(-n,x)]$.

For $\kappa=0$, only the first term, $E_1((\alpha r)^2)$, is nonzero. For $\kappa>0$ we have an alternating series, and its convergence has to be taken into account in determining the optimum value of α (in addition to the required precision and the cell size). For large values of κ, not only are a large number of terms needed in this series to reach the desired precision, the optimum value of α is also large due to convergence rquirements, increasing the cutoff in reciprocal space, so that the computation time increases dramatically. We were able to carry this calculation to $\kappa=4$, where it matched the results from the short-range method to 1 part in 20 000.

We also need the following quantities (in $d=2$):

$$\tilde{\psi}_\alpha(k)=2\pi\frac{e^{-(\kappa^2+k^2)/(2\alpha)^2}}{\kappa^2+k^2}, \quad \text{(D18)}$$

$$\lim_{k\to 0}\tilde{\psi}_\alpha(k)=\frac{2\pi}{\kappa^2}e^{-(\kappa/2\alpha)^2}, \quad \text{(D19)}$$

$$\lim_{r\to 0}\psi_\alpha(r)=\frac{1}{2}E_1\left[\left(\frac{\kappa}{2\alpha}\right)^2\right]. \quad \text{(D20)}$$

At $\kappa=0$ we take

$$\lim_{\kappa\to 0}\lim_{k\to 0}[\tilde{\psi}_\alpha(k)-\tilde{\phi}(k)]=-\frac{\pi}{2\alpha^2}. \quad \text{(D21)}$$

Also,

$$\lim_{r\to 0}\psi_\alpha(r)\approx-\gamma/2+\ln\alpha-\ln(\kappa/2)+O(\kappa^2). \quad \text{(D22)}$$

The $\ln\kappa$ term cancels in the defect energy, so that the limit $\kappa\to 0$ is again well defined. Similarly, if we did not subtract $\lim_{k\to 0}\tilde{\phi}(k)$, we would have an extra term $2\pi/\kappa^2$, which too would cancel out.

The expression for the force is similar to Eqs. (D13) where $\mathbf{f}_{ij}^R$ is a series similar to $\phi(r)-\psi_\alpha(r)$, with each $E_{n+1}((\alpha r)^2)$ replaced by $2\alpha^2E_n((\alpha r)^2)\mathbf{r}$. On scaling, $\tilde{\psi}_\alpha(k)$ has to be recalculated because it does not simply scale as a power law.

The special functions used here were all calculated to an accuracy of 10^{-16} according to routines taken from Ref. [23]. Since the power-law calculations were mostly carried out on integral values of p, the gamma functions were only needed for integral or half-integral orders, in which case certain recursion relations can be used [29]. We used the fastest method for each order.

[1] For a review of undirected living polymers, see S. A. Safran, *Statistical Thermodynamics of Surfaces, Interfaces and Membranes* (Addison-Wesley, Reading, MA, 1994), Sec. 8.

[2] E. Frey, D. R. Nelson, and D. S. Fisher, Phys. Rev. B **49**, 9723 (1994); see also, J. Prost, Liq. Cryst. **8**, 123 (1990).

[3] D. R. Nelson, in *Observation, Prediction and Simulation of Phase Transitions in Complex Fluids*, Vol. 460 of *NATO Advanced Study Institute Senes C, Mathematical and Physical Sciences*, edited by M. Baus, L. F. Rull, and J. P. Ryckaert (Kluwer Academic, The Netherlands, 1995), p. 293.

[4] S. Jain and D. R. Nelson, Macromolecules **29**, 8523 (1996).

[5] M. C. Marchetti and D. R. Nelson, Phys. Rev. B **41**, 1910 (1989).

[6] Dislocation proliferation in a supersolid phase has recently been studied by M. C. Marchetti and L. Radzihovsky, e-print cond-mat/9811193.

[7] P. Predecki and W. O. Statton, J. Appl. Phys. **37**, 4053 (1966).

[8] See, e.g., D. R. Nelson, in *Phase Transitions and Critical Phenomena*, edited by C. Domb and J. Lebowitz (Academic, New York, 1983), Vol. 7, p. 1.

[9] P.-A. Albouy, D. Guillon, B. Heinrich, A.-M. Levelut, and J. Malthête, J. Phys. II **5**, 1617 (1995).

[10] R. Podgornik, H. H. Strey, K. Gawrisch, D. C. Rau, A. Rupprecht, and V. A. Parsegian, Proc. Natl. Acad. Sci. USA **93**, 4261 (1996).

[11] J. V. Selinger and R. F. Bruinsma, Phys. Rev. A **43**, 2910 (1991).

[12] P. G. deGennes and J. Prost, *The Physics of Liquid Crystals*, 2nd ed. (Oxford University Press, Oxford, 1993).

[13] J. V. Selinger and R. F. Bruinsma, J. Phys. II **2**, 1215 (1992).

[14] See also V. G. Taratura and R. B. Meyer, Liq. Cryst. **2**, 373 (1987).

[15] M. C. Marchetti, Phys. Rev. B **43**, 8012 (1990).

[16] W. K. Kwok *et al.*, Phys. Rev. Lett. **69**, 3370 (1992).

[17] H. M. Carruzzo and C. C. Yu, Philos. Mag. B **77**, 1001 (1997).

[18] D. S. Fisher, B. I. Halperin, and R. Morf, Phys. Rev. B **20**, 4692 (1979).

[19] E. Cockayne and V. Elser, Phys. Rev. B **43**, 623 (1991).

[20] P. H. Dederichs, C. Lehmann, H. R. Schober, A. Schol, and R. Zeller, J. Nucl. Mater. **69&70**, 176 (1978).

[21] Y. Rosenfeld, Mol. Phys. **88**, 1357 (1996).

[22] D. M. Heyes, J. Chem. Phys. **74**, 1924 (1981).

[23] *Numerical Recipes*, edited by W. H. Press, B. P. Flannery, S. A. Teukolsky, and W. T. Vetterling (Cambridge University Press, New York, 1992).

[24] L. D. Landau and E. M. Lifshitz, *Theory of Elasticity* (Pergamon, New York, 1975), Sec. 7.

[25] D. J. Adams and I. R. McDonald, J. Phys. C **7**, 2761 (1974).
[26] B. R. A. Nijboer and F. W. de Wette, Physica (Amsterdam) **23**, 309 (1957).
[27] *Handbook of Mathematical Functions*, edited by M. Abramowitz and I. A. Stegun (Dover, New York, 1965).
[28] J. Medeiros e Silva and B. J. Mokross, Phys. Rev. B **21**, 2972 (1980).
[29] M. Monkenbusch, Comput. Phys. Commun. **67**, 343 (1991).